Sol–Gel Derived Inorganic–Organic Hybrid Materials Comprising Vanadia, Silica, and Thiazole Dyes

Ming-Shien Yen*
Department of Materials Engineering, Kun Shan University, Tainan 71003, Taiwan

Abstract

Herein we report the synthesis of novel vanadia/silica/thiazole azo dye inorganic–organic hybrid materials by a sol–gel process using vinyltriethoxysilane (VTES) as a precursor. The materials were synthesized from vanadia and tetraethoxysilane (TEOS) with thiazole azo dyes, which were synthesized using 2-amino thiazole as the coupling component and then underwent a coupling reaction with the diazonium component, p-nitroaniline. Alternatively, the thiazole azo dyes were processed by a hydrolysis–condensation reaction with a constant ratio of VTES, vanadia and TEOS in appropriate proportions using a catalyst. The structures of these hybrid materials were examined by Fourier transform infrared analysis, ^{29}Si nuclear magnetic resonance, X-ray diffraction, and energy-dispersive X-ray spectroscopy.

Keywords—*vanadia, silica, thiazole dyes, hybrid materials*

I. INTRODUCTION

Traditional materials with a single-function have been gradually replaced by multifunctional, eco-friendly materials that can improve human health and add value to products [1-4]. Inorganic–organic composite materials with well-defined nanostructures have gained interest because of their improved properties resulting from the combination of two components into one uniform material [5]. Organic–inorganic hybrid materials include ceramic and polymer materials with multiple complementary functions. The ceramic materials have very high strengths and heat resistance, whereas the polymer materials have good toughness and processing properties. Generally, organic-inorganic hybrid materials have been fabricated using the sol–gel and intercalation processes. The sol–gel composite manufacturing approach is suitable for many types of materials and process more variability [6-8].

The sol–gel process is commonly used for preparing inorganic–organic hybrid materials. This process increases the interaction between the inorganic and organic components while allowing the inorganic phase to achieve nanometer-size dimensions. Hybrid materials have superior toughness and working quality because of the organic component, and rigidity, dimensions, and thermal stability because of the inorganic component. The inorganic and organic components can be integrated to form a homogeneous biphase system via chemical bonds between the organic and inorganic phases [9-12]. Metal alkoxides are very sensitive to hydrolysis due to the low reactivity of tetra-alkoxysilanes. This synthesis method can be used for the preparation of many inorganic materials, including TiO_2, SiO_2, ZrO_2, V_2O_5, and Al_2O_3 [13-18].

Vanadium oxides, such as VO_2, V_2O_3, and V_2O_5, have been widely studied as materials for use in many applications because of their outstanding photochromic [19], thermochromic [20], electrospinning [21, 22], and electrochromic display [23, 24] properties. Therefore, significant efforts have been focused on these properties for applications in fields including catalysis [25-27], chemical sensors [28], fuel cells [29], conductive electrodes [30, 31], anode materials for symmetric supercapacitors [32], lithium ion batteries [33-35], and gasochromic smart windows [36, 37]. Vanadium pentoxide is a transition metal oxide with a layered structure. Its special structure results in excellent electrical conductivity, electrochromism, and temperature resistance, and particular electronic, ionic, semiconducting, and electrochemical properties [38, 39]. The fascinating properties and wide application range of vanadia thin films have attracted significant attention over the past decades. These properties include its wide optical band gap, layered structure, good chemical and thermal stability, and excellent thermoelectric and electrochromic properties. Practical applications of vanadia thin films have been reported, including optical-switching devices [40, 41], energy storage and conversion [42], smart windows [43], electrochromic devices [44–46], and superhydrophobic nanowires [47].

Furthermore, silica is a natural material derived from common materials such as quartz, sand, and flint. Silica has high chemical stability, a low thermal expansion coefficient, and high heat resistance. The relatively high chemical stability of the silica phase can be advantageous in some cases [48–51]. Among

metal compounds, vanadia possesses unusual physicochemical properties and electrical activities. Moreover, if vanadia and silica gels are sufficiently intermixed within the surface layer of a material during the condensation polymerization process, the short travelling distance between the surface-modified silica sites provides thermal stability, and the vanadia sites provide electrical properties.

The molecules of heteroaryl azo dyes contain unshared electron pairs of nitrogen and sulfur that can easily trigger resonance and cause the excitation of π electrons of the compound from the ground state to the excited state. The synthesis and spectroscopic properties of azo dyes are well-established [52–56]. The use of heterocyclic aromatic amines to improve the tinctorial strength has been well established. Unlike analogous dyes derived from benzenoid compounds, 2-aminothiazole compounds, which possess different substituents in the 4-position of the analogous derivatives as diazo components, tend toward bathochromic shifts [57–59].

Modern industries and consumers desire multifunctional products; therefore, multifunctioning organic–inorganic hybrid materials have become popular. The sol–gel method is a frequently used organic–inorganic hybrid material preparation method that combines inorganic and organic molecular networks. Vanadium-containing oxide materials obtained by sol–gel synthesis yielded a transparent solid gel and are expected to find wide practical application. Vanadia can be used to increase the functionality of hybrid materials. The use of the vanadia precursor, which was subsequently incorporated in other organic material syntheses to create hybrid materials that are widely used to produce various chemical products. The vanadia network structure was combined with a siloxane network to increase the additive effect, thereby obtaining heat accumulation capabilities and superhydrophobicity. Subsequently, the sol–gel method was applied to prepare organic–inorganic hybrid dyes, which yielded hybrid materials that exhibited a network structure consisting of the processed dye, VTES(vinyltriethoxysilane) /vanadia, and VTES/TEOS(tetraethoxysilane)/vanadia through additive hydrolysis. This will enable the use of hybrid dyes when processing high molecular products.

II. EXPERIMENT

A. Analytical Instruments

Fourier-transform infrared (FT-IR) spectra were measured using a Bio-Rad Digilab FTS-40 spectrometer (KBr). ^{1}H nuclear magnetic resonance (NMR) spectra were obtained using a BRUKER ADVANCE 400MHz NMR spectrometer. Chemical shifts (δ) are expressed in parts per million using tetramethylsilane (TMS) as an internal standard. The ^{29}Si-NMR spectra were collected using a BRUKER ADVANCE 400 MHz NMR spectrometer at 78.49 MHz, with a recycle time of 60 s, and the number of scans was 914. The elemental analysis was performed using a Philips XL40 FEG-Energy Dispersive X-ray Spectrometer. X-ray diffraction (XRD) measurements were performed on a Rigaka D/MAX 2500V X-ray powder diffractometer in steps of 0.01° using Cu K_{α} radiation as the X-ray source.

B. Materials

Vinyltriethoxysilane (VTES), tetraethoxysilane (TEOS), p-nitroaniline, ammonium metavanadate, and acetophenone were purchased from Acros Co., Ltd., Belgium. Thiourea, sulfuric acid, and iodide were purchased from Hayashi Pure Chemical Ind., Ltd., Japan.

C. Preparation of dye 5-[2-(4-nitrophenyl)-diazen-1-yl]-4-phenyl-1,3-thiazol- 2-amine (3)

A finely ground powder of *p*-nitroaniline **2** (1.38 g, 0.01 mol) was added to hydrochloric acid (12 mL) and stirred for 20 min. Sodium nitrite (0.72 g, 0.0105 mol) was added in portions to concentrated sulfuric acid (5 mL) at 10 °C and stirred for 1 h at 60–65 °C. The solution was cooled to below 5 °C, and then the finely ground derivatives were slowly added; the mixture was stirred for an additional 1 h at 5–10 °C until it was clear. The resulting diazonium solution was used immediately in the coupling reaction. A clear mixed solution of the coupling component 4-phenyl-2-aminothiazole **1** (2.0 g, 0.01 mol) and 10% sodium carbonate was stirred. The diazonium mixture was added at 0–5 °C, and the solution was stirred for at least 2 h; it was diluted to raise its pH to 5–6 (by adding aqueous sodium hydroxide or sodium acetate). The resulting product was filtered, washed with water, and re-crystallized from ethanol to give a deep red solid, 5-[2-(4-nitrophenyl)-diazen-1-yl]-4-phenyl-1,3-thiazol-2-amine (**3**) (2.3 g, 70%). M.P. 245-247 °C; Fourier transform infrared (FT-IR) (KBr)/cm^{-1}: 3433 (NH_2), 3057 (C–H); ^{1}H NMR (DMSO-d_6) δ ppm: 7.04 (1H, s, –NH_2), 7.51–7.55 (5H, m, ArH), 7.71, (2H, d, 2,6- Ph–H), 8.19 (2H, d, 3,5- Ph–H). $C_{15}H_{17}N_2O_2S$ (325.1) Calcd.: C, 55.38; H, 3.41; N, 21.53; O, 9.84; S, 9.85. Found: C, 55.32; H, 3.44; N, 21.58; O, 9.78; S, 9.87.

D. Preparation of precursor 5-[2-(4-nitrophenyl)-diazen-1-yl]-4-phenyl-N-[2- (triethoxysilyl)ethyl]-1,3- thiazol-2-amine (4)

Precursor **4** was prepared by the reaction of dye **3** (3.25 g, 0.01 mol) followed by the addition of VTES (9.5 g, 0.05 mol) in ethanol (80 mL) while stirring at 65 °C for 4 h at an adjusted pH of 4–5. The resulting product was filtered, washed with water, and re-crystallized from ethanol to give a dark red solid, 5-[2-(4-nitrophenyl)-diazen-1-yl]- 4-phenyl-N-[2-(triethoxysilyl)ethyl]-1,3-thiazol-2-amine (**4**) (2.76 g, 59%). M.P. 304–306 °C; FT-IR (KBr)/cm^{-1}: 3395

(NH), 3073 (C–H), 1096 (O–Si). $C_{23}H_{29}N_5O_5SSi$ (515.4) Calcd.: C, 53.57; H, 5.67; N, 13.58; O, 15.51; S, 6.22; Si, 5.45. Found: C, 53.63; H, 5.62; N, 13.56; O, 15.55; S, 6.28; Si, 5.41.

E. Preparation of vanadia

For preparing the vanadia precursor, 1.69 g (0.01 mol) ammonium metavanadate was used as the raw material and mixed with 30 ml of ethylene glycol as the solvent. The reaction system was irradiated by a halogen lamp and mixed at 270 ℃ for reaction. The ammonium metavanadate reacted with ethylene glycol to generate vanadic alkoxide, then a hydrolytic reaction occurs to form the vanadia precursor. The reaction is described in Scheme 1.

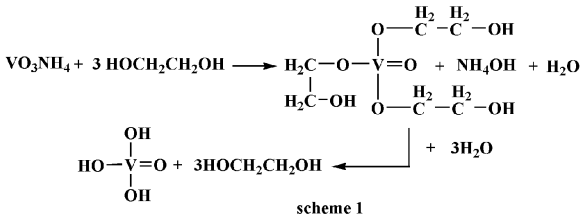

scheme 1

Scheme 1 Synthesis of vanadia precursor

F. Synthesis of hybrid materials

As shown in Scheme 2, precursor **4** and the prepared vanadia precursor were mixed in a fixed ratio. To this was added 0.01 mol of hydrochloric acid and 10 mL of water to maintain a pH level of 3–4. The mixture was then placed in a thermostat stirrer and heated under reflux for 4 h to facilitate a condensation reaction to produce a hybrid material. We changed the concentration of the vanadia precursor in the prepared solution doped with TEOS to attain varying degrees of the polycondensation reaction and obtain hybrid materials **5** and **6**. The reaction is described in Scheme 2.

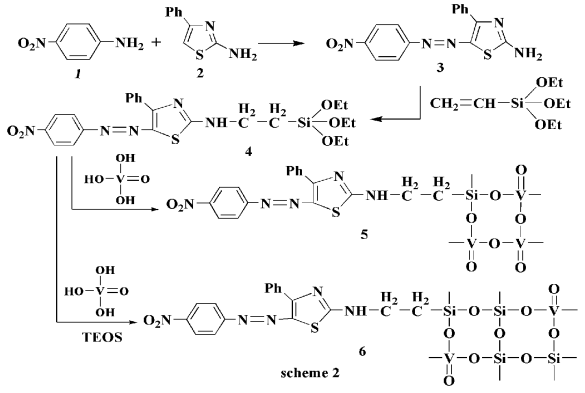

scheme 2

Scheme 2 Synthesis of hybrid material 5, 6

G. Preparation of hybrid materials

Hybrid material $\mathbf{V_1}$ was prepared by the condensation of precursor **4** (5.01 g, 0.01 mol) and the prepared vanadia precursor (0.02 mol) in ethanol (80 mL) by stirring at 65 °C for 2 h with the addition of hydrochloric acid (0.365 g, 0.01 mol) and water (5 mL). Hybrid materials $\mathbf{V_2}$–$\mathbf{V_4}$ were synthesized using the same method as that used for synthesizing $\mathbf{V_1}$; however, the molar ratios of precursor **4** to the vanadia precursor were 1:2, 1:4, 1:6, and 1:8 for the hybrid materials $\mathbf{V_1}$–$\mathbf{V_4}$, respectively. Hybrid material $\mathbf{Z_1}$ was prepared by the condensation of precursor **4** (5.01 g, 0.01 mol), TEOS (4.16 g, 0.025 mol), and vanadia precursor (0.04 mol) in ethanol (80 mL) while stirring at 65 °C for 2 h by adding hydrochloric acid (0.365 g, 0.01 mol) and water (5 mL). The **Z** series of hybrid materials were synthesized using the same method but with different molar ratios of precursor **4** to TEOS during hydrolysis polycondensation at a constant ratio of vanadia precursor; the molar ratios of precursor **4**:TEOS:vanadia precursor were 1:2.5:4, 1:5:4, 1:7.5:4, and 1:10:4 for $\mathbf{Z_1}$–$\mathbf{Z_4}$, respectively. Hybrid material $\mathbf{X_1}$ was prepared by the condensation of precursor **4** (5.01 g, 0.01 mol), TEOS (4.16 g, 0.1 mol), and vanadia precursor (0.02 mol) in ethanol (80 mL) while stirring at 65 °C for 2 h and adding hydrochloric acid (0.365 g, 0.01 mol) and water (5 mL). The **X** series of hybrid materials were prepared by the same method but with different molar ratios of precursor **4** to vanadia precursor during hydrolysis polycondensation at a constant ratio of TEOS; the molar ratios of precursor **4**:TEOS:vanadia precursor were 1:10:2, 1:10:4, 1:10:6, and 1:10:8 for $\mathbf{X_1}$–$\mathbf{X_4}$, respectively.

III. RESULTS AND DISCUSSION

A. FTIR analysis

The FTIR spectra of the dyes and hybrid materials indicate that dye **3** has absorption peaks corresponding to the N–H and C–H groups at 3332 and 2972 cm^{-1}, respectively. In the FTIR spectrum of precursor **4**, an obvious shift in the amino group absorption peak close to 3424 cm^{-1}, which is typically found at 3418 cm^{-1}, suggests partial reaction of the dye with VTES. The appearance of the Si–OR absorption peak around 1074 cm^{-1} proves that VTES could convert the primary amine group into a secondary amine group; the resultant absorption peak appeared around 3380 cm^{-1}. These results indicate reactions between some of the dyes and VTES. The FTIR spectrum of hybrid material **6** includes the absorption peak of the converted secondary amine. The intense signal corresponding to the Si–O group at 1100 cm^{-1} proves the dissociation of the NH_2 moiety. The Si–C bond, which gave rise to the peak at 1244 cm^{-1}, reveals that the dissociation of NH_2 bond is followed by bonding with CH_2, resulting in the linkage of the Si–O bonds to form Si–O–Si network.

The hybrid materials $\mathbf{V_1}$–$\mathbf{V_4}$ were analyzed using FT-IR. Figure 1 shows a N-H group absorption peak near 3429 cm^{-1}, C-H group near 3175 cm^{-1}, and C=C group absorption peak near 1638 cm^{-1}. There is also a Si-O group absorption peak near 1120 cm^{-1} and V=O group absorption peak near 982 cm^{-1}. The V=O group absorption peak size increases as the concentration

increases. The hybrid materials **Z_1–Z_4** were analyzed by FT-IR. Figure 2 shows a N-H group absorption peak near 3480 cm^{-1}, a C=C group absorption peak near 1680 cm^{-1}, a V=O group absorption peak near 966 cm^{-1}, and Si-O group absorption peak near 1061 cm^{-1}. It was observed that after the TEOS was applied, the absorption peaks of the N-H and C=C groups shifted left and the Si-O group absorption peak size noticeably increased, whereas the V=O group absorption peak size decreased gradually. The vanadium pentoxide precursor concentration in the hybrid material decreased by the addition of TEOS, so the V=O group absorption peak size decreased. The hybrid materials **X_1–X_4** were analyzed using FT-IR. Figure 3 shows a N-H group absorption peak near 3429 cm^{-1}, C=C group absorption peak near 1638, Si-O group absorption peak near 1082 cm^{-1}, and V=O group absorption peak near 963 cm^{-1}. The hybrid material **X_2** had the most apparent Si-O and V=O group absorption peaks, followed by hybrid material **X_3**. This suggests that the hybrid material **X_2** has more network structures.

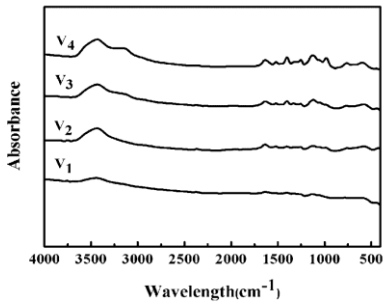

Fig. 1 FT-IR spectra of hybrid materials V_1–V_4

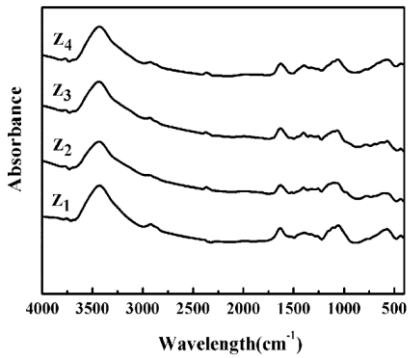

Fig. 2 FT-IR spectra of hybrid materials Z_1–Z_4

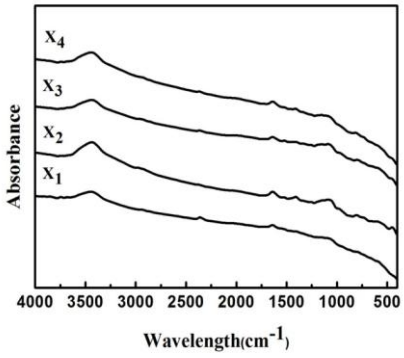

Fig. 3 FT-IR spectra of hybrid materials X_1–X_4

B. ^{29}Si NMR spectra analysis

^{29}Si NMR is often used to characterize the structures formed by Si hydrolysis. While the FTIR results above indicated the formation of Si–O–Si bonds by a sol–gel reaction, the solid-state ^{29}Si NMR provided additional information on the structure of silica and the extent of the Si–OH condensation reaction. The T^3, Q^3, and Q^4 absorption peaks were located by applying ^{29}Si NMR spectroscopy. Figure 4 shows that the ^{29}Si NMR spectra of the simple dye and VTES contain absorption peaks at ~78.47 ppm (T^3), corresponding to Si–OR formation following the hydrolysis of VTES. Figure 5 shows the ^{29}Si NMR spectra of the processed hybrid dye formed with various proportions of VTES and TEOS. Peaks appeared at ~100.37 ppm (Q^3) owing to absorption by $(H–O)Si(–OSi\equiv)_3$ structures and at ~109.22 ppm (Q^4) due to the absorption by $Si(–OSi\equiv)_4$ structures. The structure of the Si–OR absorption peak indicated that some Si quadruple bonds had an unreacted Si–OH functional group, $(H–O)Si(–OSi\equiv)_3$, and some Q^3 quadruple bonds had an unreacted Si–O functional group, $Si(–OSi\equiv)_3$. The structure of Q^4 indicates that the Si quadruple bond reacted completely with the Si–O functional group, $Si(–OSi\equiv)_4$.

Hybrid material **V_2**, prepared by a polycondensation reaction of precursor **4** and fixed proportions of vanadia precursor was analyzed using ^{29}Si-NMR (nuclear magnetic resonance spectrum). Figure 4 shows that the noise peak is relatively significant in the analysis chart, and there is an apparent T^3 absorption peak at δ: -78.47 ppm. The hybrid material may existe as $R\text{-}Si(\text{-}OSi\equiv)_3$, meaning that the hybrid material did not form an Si-O-Si network structure, but it is known that the precursor and vanadia combined to form hybrid material **V_2**.

The hybrid material prepared by fixing the vanadia precursor proportion and changing the concentration of TEOS was analyzed using ^{29}Si-NMR. Figure 5 shows that a hybrid material network structure formed, as there are Q^3 and Q^4 absorption peaks besides T^3 absorption peak. In the spectra of the hybrid materials **Z_1–Z_4**, the T^3 absorption peak occurs near δ: -78.47 ppm and decreases in size as the TEOS concentration increases. This may be because the hybrid material network structure forms a Si-O-Si network structure as the concentration increases, contributing to the decline of the $R\text{-}Si(\text{-}OSi\equiv)_3$ structure, so that the T^3 absorption peak decreases in size accordingly. The absorption peak Q^3 decreases in size as the concentration increases near δ: -100.37 ppm because the hybrid material network structure has V=O bonding, and the bonding between vanadia and Si-O groups decreases, so that the Q^3 absorption peak size decreases at δ: -100.37 ppm. For the existence of V=O bonding, the hybrid material is unlikely to form large-scale network structure, the absorption peak Q^4 becomes more apparent as the TEOS concentration increases, and it occurs near δ: -

109.22 ppm, indicating that the hybrid material network structure is more complete.

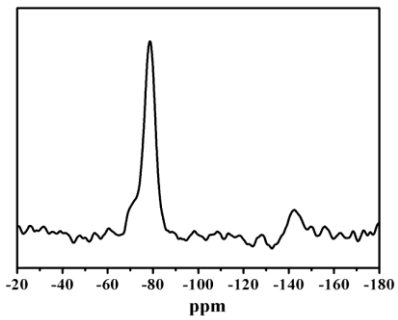

Fig. 4 ^{29}Si-NMR spectra of hybrid material V_2

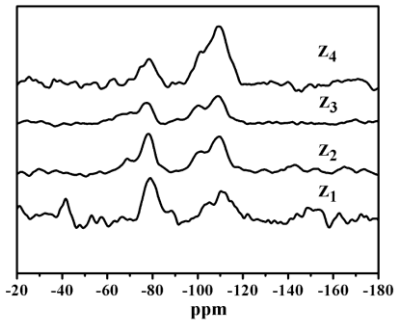

Fig. 5 ^{29}Si-NMR spectra of hybrid materials Z_1–Z_4

C. Energy-dispersive X-ray spectra analysis

The energy-dispersive X-ray spectroscopy (EDS) analysis results are presented in Table 1 and Figures 6 and 7. When additional vanadia precursor was added to hybrids $\mathbf{V_1}$ and $\mathbf{V_3}$, the quantity of Si decreased with increase in vanadium concentration. As shown in Table 1 and Figures 8 and 9, the hybrids $\mathbf{Z_1}$ and $\mathbf{Z_3}$ had a fixed molar concentration of vanadia precursor and a moderately increased molar concentration of TEOS. EDS analysis showed that the increasing TEOS concentration increased the V content in the hybrid materials, and thus, the vanadia precursor concentration decreased gradually. In hybrid materials $\mathbf{X_1}$ and $\mathbf{X_3}$, according to the results in Table 1 and Figures 10 and 11, the V content increased with vanadia precursor addition.

Table 1: EDS analysis of hybrid materials V_1–V_4, Z_1–Z_4, and X_1–X_4

Samples	Elemental composition (%)				
	C	O	S	Si	V
$\mathbf{V_1}$	34.40	18.19	7.25	20.04	20.12
$\mathbf{V_2}$	30.34	19.21	7.20	20.10	23.15
$\mathbf{V_3}$	21.85	19.57	6.56	20.19	30.83
$\mathbf{V_4}$	18.64	20.25	5.20	20.22	35.69
$\mathbf{Z_1}$	28.17	18.16	4.81	20.64	28.22
$\mathbf{Z_2}$	26.83	18.53	3.50	27.24	23.90
$\mathbf{Z_3}$	25.45	18.64	3.15	30.98	21.78
$\mathbf{Z_4}$	23.79	19.03	2.94	33.79	20.45
$\mathbf{X_1}$	30.74	19.44	3.36	26.36	20.10
$\mathbf{X_2}$	23.36	25.85	2.50	26.72	21.57
$\mathbf{X_3}$	20.97	21.50	2.17	27.10	28.26
$\mathbf{X_4}$	17.84	14.42	1.93	29.83	35.98

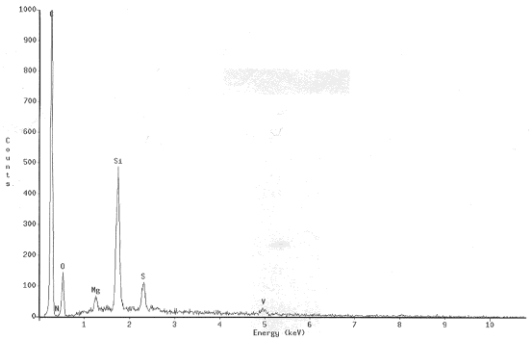

Fig. 6 The EDS diagram of hybrid materials V_1

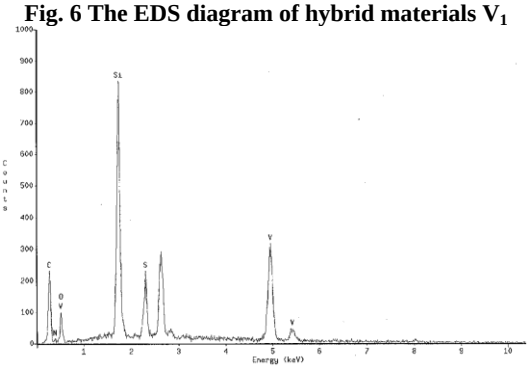

Fig. 7 The EDS diagram of hybrid materials V_3

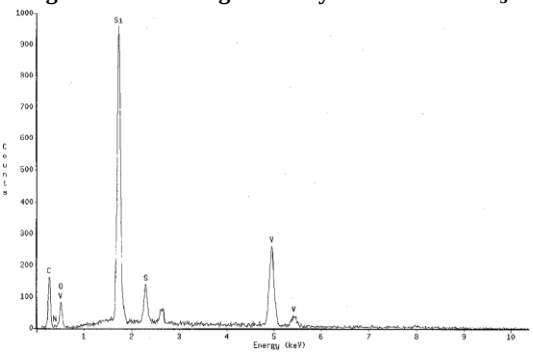

Fig. 8 The EDS diagram of hybrid materials Z_1

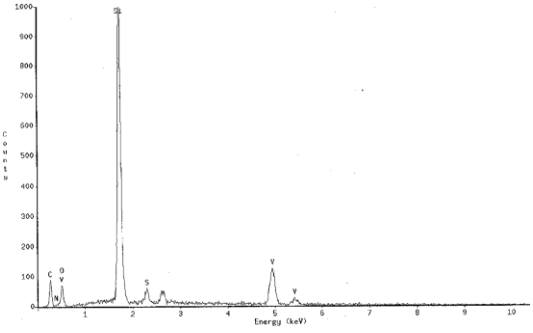

Fig. 9 The EDS diagram of hybrid materials Z_3

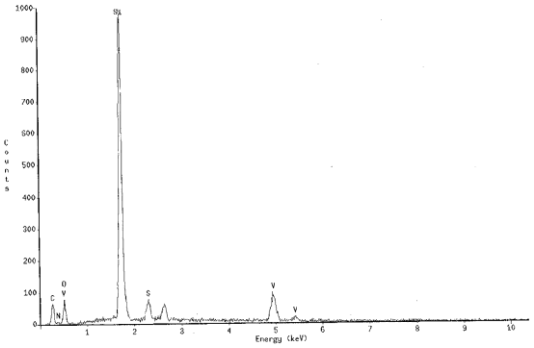

Fig. 10 The EDS diagram of hybrid materials X_1

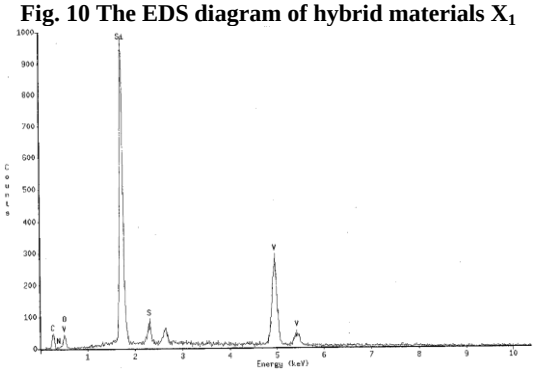

Fig. 11 The EDS diagram of hybrid materials X_3

D. X-Ray diffraction analysis

In this study, we analyzed hybrid materials $\mathbf{V_4}$ and the un-sintered vanadia powder developed by a sol–gel process (hereafter, vanadia powder) using X-ray diffraction (XRD). Because neither the series of hybrid materials nor the vanadia powder was sintered, all these materials exhibited amorphous structures without clear crystal phases, as shown in Figure 12. Figure 12 shows the XRD spectrum of the V crystal structure, with the prominent peak at 2θ = 26.97°, corresponding to the (111) Bragg's reflections of an FCC crystal structure. Figure 13 shows the light diffraction analysis of hybrid material $\mathbf{V_4}$ prepared with precursor **4**, TEOS, and vanadia, in which the peaks appeared at 2θ = 25.14°. The peak near 2θ = 25.14° may be the peak of the dye, while the other peaks correspond to V metal in the hybrid material, approximately matching data from literature. The noise peaks in the spectrum of the hybrid material arose because the dye has an amorphous structure and its peak was not obvious.

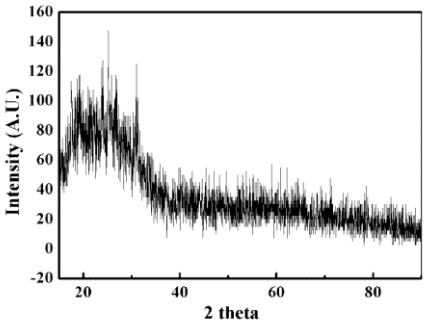

Fig. 12 The XRD diagram of hybrid materials V_4

IV. CONCLUSIONS

This study was primarily focused on the sol–gel synthesis of a series of heterocyclic thiazole dyes with various proportions of added VTES/vanadia and VTES/TEOS/vanadia. The derived hybrids were further analyzed to understand their chemical and physical properties. FT-IR analysis showed that the absorption peak of the Si–O–Si functional group appeared in the range of 1061 to 1120 cm^{-1}, which confirmed the formation of a network structure. In the ^{29}Si-NMR analysis, the Q^3 peak appeared near δ= -100.37 ppm for hybrid materials $\mathbf{Z_1}$–$\mathbf{Z_4}$ but disappeared gradually as the bonding between vanadia and Si-O groups decreased. Moreover, only the Q^4 absorption peak appeared near δ= -109.22 ppm as the TEOS concentration increased. In addition, the EDS results showed that when additional vanadia was added to hybrids $\mathbf{X_1}$–$\mathbf{X_4}$, the increased vanadia content led to a continuous decrease in the Si content. Furthermore, the peaks of V in hybrid material $\mathbf{V_4}$ appeared at 2θ = 25.14°.

ACKNOWLEDGMENT

The authors thank the Ministry of Science and Technology of the Republic of China, Taiwan, for financially supporting this research under grant MOST 106-2221-E-168-026.

REFERENCES

[1] T.Matsuo, "Advanced technical textile products," Text. Prog., vol. 40(3), pp. 123–181, 2008.
[2] M.Mohseni, P. F. James, and P. V. Wright, "Vanadium-Based Organic-Inorganic Hybrid Materials Prepared by a Sol-Gel Method," J. Sol-Gel Sci. Technol., vol. 13, pp. 495–497, 1998.
[3] K.Qi, J. H. Xin, W. A. Daoud, and C. L. Mak, "Functionalizing Polyester Fiber with a Self-Cleaning Property Using Anatase TiO_2 and Low-Temperature Plasma Treatment," Int. J. Appl. Ceram. Technol., vol. 4(6), pp. 554–563, 2007.
[4] R.Kotek, "Recent Advances in Polymer Fibers," Polym. Rev., vol. 48, pp. 221–229, 2008.
[5] C.Sanchez, B. Julian, P. Belleville, and M. Popall, "Applications of hybrid organic–inorganic nanocomposites," J. Mater. Chem., vol. 15, pp. 3559–3592, 2005.
[6] S.Vives and C. Meunier, "Mixed SiO_2–TiO_2 (1:1) sol–gel films on mild steel substrates Sol composition and thermal treatment effects," Surf. Coat. Tech., vol. 202, pp. 2374–2378, 2008.
[7] Z.Liu, X. Zhang, T. Murakami, and A. Fujishima, "Sol–gel SiO_2-TiO_2 bilayer films with self-cleaning and antireflection properties," Sol. Energ. Mat. Sol. C., vol. 92: pp. 1434–1438, 2008.
[8] A.A. Herrero, G. Ramos, F. D. Monte, E. Bernabeu, and D. Levy, "Water adsorption in porous TiO_2–SiO_2 sol–gel films analyzed by spectroscopic ellipsometry," Thin Solid Films, vol. 455, pp. 356–360, 2004.
[9] P.Judeinstein and C. Sanchez, "Hybrid organic inorganic materials a land of multidisciplinarity," J. Mater. Chem., vol. 6, pp. 511–525, 1996.
[10] L.Matejka, O. Dukh, and J. Kolarik, "Reinforcement of crosslinked rubbery epoxies by in-situ formed silica," Polymer, vol. 41, pp. 1449–1459, 2000.
[11] W.Zhou, J. E. Mark, M. R. Unroe, and F. E. Arnold, "Toughening of a high-temperature polymer by the sol–gel, in

situ generation of a rubbery silica–siloxane phase," J. Appl. Polym. Sci., vol. 79, pp. 2326–2330, 2001.
[12] C.L. Jackson, B. J. Bauer, and A. I. Nakatani, "Synthesis of Hybrid Organic−Inorganic Materials from Interpenetrating Polymer Network Chemistry," Chem. Mater., vol. 8, pp. 727–733, 1996.
[13] Z.Jiwei, Y. Taob, Z. Liangying, and Y. Xia, "The optical waveguiding properties of TiO_2–SiO_2 composite films prepared by the sol–gel process," Ceram. Int., vol. 25, pp. 667–670, 1999.
[14] D.S. Hinczewski, M. Hinczewski, F. Z. Tepehan, and G. G. Tepehan, "Optical filters from SiO_2 and TiO_2 multi-layers using sol–gel spin coating method," Sol. Energ. Mater. Sol. C., vol. 87, pp. 181–196, 2005.
[15] B.Tyagi, K. B. Sidhpuria, B. Shaik, and R. V. Jasra, "Effect of Zr-Si molar ratio and sulfation on structural and catalytic properties of ZrO_2–SiO_2 mixed oxides," J. Porous Mater., vol. 17, pp. 699–709, 2010.
[16] J.Livage, G. Guzman, and F. Bételle, "Optical properties of sol-gel derived vanadium oxide films," J. Sol-Gel Sci. Technol., vol.8, pp. 857–865, 1997.
[17] R.Linacero, M. L. Rojas-Cervantes, and J. D. D. Lopez-Gonzalez, "Preparation of $xTiO_2$ $(1-x)Al_2O_3$ catalytic supports by the sol-gel method: physical and structural characterization," J. Mater. Sci., vol. 35, pp. 3279–3287, 2000.
[18] S.Sivakumar, C. P. Sibu, P. Mukundan, P. K. Pillai, and K. G. K. Warrier, "Nanoporous titania–alumina mixed oxides—an alkoxide free sol-gelsynthesis," Mater. Lett., vol. 58, pp. 2664–2669, 2004.
[19] Z.Liu, G. Fang, Y. Wang, Y. Bai, and K. L. Yao, "Laser-induced colouration of V_2O_5," J. Phys. D: Appl. Phys., vol. 33, pp. 2327–2332, 2000.
[20] F.Béteille and J. Livage, "Optical Switching in VO_2 Thin Films," J. Sol-Gel Sci. Technol., vol. 13, pp. 915–921, 1998.
[21] O.Ya. Berezina, D. A. Kirienko, N. P. Markova, and A. L. Pergament, "Synthesis of Vanadium Pentoxide Micro and Nanofibers by Electrospinning," Tech. Phy., Vol. 60(9), pp. 1361–1366, 2015.
[22] P.Viswanathamurthi, N. Bhattarai, H. Y. Kim, and D. R. Lee, "Vanadium pentoxide nanofibers by electrospinning," Scripta Mater., vol. 49, pp. 577–581, 2003.
[23] Y.Liu, C. Jia, Z. Wan, X. Weng, J. Xie, and L. Deng, "Electrochemical and electrochromic properties of novel nanoporous NiO/V_2O_5 hybrid film," Sol. Energ. Mater. Sol. C., vol. 132, pp. 467–475, 2015.
[24] M.Alsawafta, A. Almoabadi, S. Badilescu, and V. V. Truong, "Improved Electrochromic Properties of Vanadium Pentoxide Nanorods Prepared by Thermal Treatment of Sol-Gel Dip-Coated Thin Films," J. Electrochem. Soc., vol. 162 (7) pp. H466-H472, 2015.
[25] H.R. Patil and Z. V. P. Murthy, "Vanadium-Doped Magnesium Oxide Nanoparticles Formation in Presence of Ionic Liquids and Their Use in Photocatalytic Degradation of Methylene Blue," Acta Metall. Sin. (Engl. Lett.), vol. 29(3), pp. 253–264, 2016.
[26] Y.o Li, J. L. Kuang, Y. Lu, and W. B. Cao, "Facile Synthesis of Flower-Like V2O5 Powders and their Photocatalyst Behavior," Acta. Metall. Sin. (Engl. Lett.), vol. 30(10), pp. 1017–1026, 2017.
[27] R.Jaiswala, N. Patelb, D. C. Kotharia, and A. Miotello, "Improved visible light photocatalytic activity of TiO_2 co-doped with Vanadium and Nitrogen," Appl. Catal. B: Environ., vol. 126, pp. 47–54, 2012.
[28] Y.Qina, M. Cuia, and Z. Yeaa, "Adsorption of ethanol on V_2O_5 (010) surface for gas-sensing applications: Ab initio investigation," Appl. Surf. Sci., vol. 379, pp. 497–504, 2016.
[29] Á.Realpe, Y. Pino, and M. T. Acevedo, "Synthesis of a Proton Exchange Membrane from Natural Latex Modified with Vanadium Pentoxide for Application in a Fuel Cell," Inter. J. Chem. Tech. Res., Vol.9(6), pp. 524–529, 2016.
[30] R.S. Ingole and B. J. Lokhande, "Electrochemical properties of dip-coated vanadium pentaoxide thin films," Bull. Mater. Sci., Vol. 39(6), pp. 1603–1608, 2016.
[31] G.T. Mola, E. A. A. Arbab, B. A. Taleatu, K. Kaviyarasu, I. Ahmad, and M. Maaza, "Growth and characterization of V_2O_5 thin film on conductive electrode," J. Microsc., Vol. 265(2), pp. 214–221, 2017.
[32] Y.Yang, K. Shen, Y. Liu, Y. Tan,. X. Zhao, J. Wu, X. Niu, and F. Ran, "Novel Hybrid Nanoparticles of Vanadium Nitride Porous Carbon as an Anode Material for Symmetrical Supercapacitor," Nano-Micro Lett., vol. 9(6), pp. 1–15, 2017.
[33] J.Wu, I. Byrd, C. Jin, J. Li, H. Chen, T. Camp, R. Bujol, A. Sharma, and H. Zhang, "Reinvigorating Reverse-Osmosis Membrane Technology to Stabilize the V2O5 Lithium-Ion Battery Cathode," Chem. Electro. Chem., vol. 4, pp. 1181–1189, 2017.
[34] D.McNulty, D. N. Buckley, and C. O. Dwyer, "Synthesis and electrochemical properties of vanadium oxide materials and structures as Li-ion battery positive electrodes," J. Power Sources, vol. 267, pp. 831–873, 2014.
[35] Y.Liu, W. Zhong, Y. Du, Q. X. Yuan, X. Wang, and R. Jia, "Novel radial vanadium pentoxide nanobelt clusters for Li-ion batteries," J. Alloys Compd., vol. 633, pp. 353–358, 2015.
[36] W.Feng, L. Zou, G. Gao, G. Wu, J. Shen, and W. Li, "Gasochromic smart window optical and thermal properties, energy simulation and feasibility analysis," Sol. Energ. Mater. Sol. C., vol. 144, pp. 316–323, 2016.
[37] J.L. Chen et al., "Behind the color switching in gasochromic VO_2," Phys. Chem. Chem. Phys., vol. 17, pp. 3482–3489, 2015.
[38] J.Livage, "Vanadium Pentoxide Gels," Chem. Mater., vol. 3, pp. 578–593, 1991.
[39] M.G. Kanatzidis and C. G. Wu, "Conductive Polymer Bronzes. Intercalated Polyaniline in V_2O_5 Xerogels," J. Am. Chem. Soc., vol. 111(11), pp. 4139–4141, 1989.
[40] F.Bételle and J. Livage, "Optical Switching in VO_2 Thin Films," J. Sol-Gel Sci. Technol., vol. 13, pp. 915–921, 1998.
[41] S.B. Zhang, D. W. Zuo, and W. Z. Lu, "Influence of film thickness on structural and optical-switching properties of vanadium pentoxide films," Surf. Eng., vol. 33(4), pp. 292–298, 2017.
[42] A.Mauger and C. M. Julien, "V_2O_5 thin films for energy storage and conversion," AIMS Mater. Sci., vol. 5(3), pp. 349–401, 2018.
[43] L.Y. L. Wu, Q. Zhao, H. Huang, and R. J. Lim, "Sol-gel based photochromic coating for solar responsive smart window," Surf. Coat. Technol., vol. 320, pp. 601–607, 2017.
[44] M.Benmoussa, A. Outzourhit, A. Bennouna, and E. L. Ameziane, "Electrochromism in sputtered V_2O_5 thin films structural and optical studies," Thin Solid Films, vol. 405, pp. 11–16, 2002.
[45] R.Ceccato, and G. Carturan, "Sol–Gel Synthesis of Vanadate-Based Thin Films as Counter Electrodes in Electrochromic Devices," J. Sol-Gel Sci. Technol., vol. 26, pp. 1071–1074, 2003.
[46] A.Cremonesi, D. Bersani, P. P. Lottici, Y. Djaoued, and R. Brüning, "Synthesis and structural characterization of mesoporous V_2O_5 thin films for electrochromic applications," Thin Solid Films, vol. 515, pp. 1500–1505, 2006.
[47] K.Senthila, G. Kwak, and K. Yong, "Fabrication of superhydrophobic vanadium pentoxide nanowires surface by chemical modification," Appl. Surf. Sci., vol. 258, pp. 7455–7459, 2012.
[48] W.Zhou, J. E. Mark, M. R. Unroe, and F. E. Arnold, "Toughening of a high-temperature polymer by the sol–gel, in situ generation of a rubbery silica–siloxane phase," J. Appl. Polym. Sci., vol. 79, pp. 2326–2330, 2001.
[49] N.D. Hegde and A. V. Rao, "Physical properties of methyltri-methoxysilane based elastic silica aerogels prepared by the two-stage sol–gel process," J. Mater. Sci., vol. 42, pp. 6965–6971, 2007.
[50] Y.Dimitriev, Y. Ivanova, and R. Iordanova," History of sol–gel science and technology," J. Univ. Chem. Technol. Metall., vol. 43(2), pp. 181–192, 2008.
[51] X.Du and J. He, "A self-templated etching route to surface-rough silica nanoparticles for superhydrophobic coatings," ACS Appl. Mater. Interfaces, vol. 3, pp. 1269–1276, 2011.
[52] A.D. Towns, "Developments in azo disperse dyes derived from heterocyclic diazo components," Dyes Pigm., vol. 42, pp. 3–28, 1999.

[53] I.Zadrożna and E. Kaczorowska, "Synthesis and absorption spectra of hetarylazo dyes derived from coupler 4-aryl-3-cyano-2-aminothiophenes," Dyes Pigm., vol. 71, pp. 207–211, 2006.
[54] M.S. Yen and I. J. Wang, "A facile syntheses and absorption characteristics of some monoazo dyes in bis-heterocyclic aromatic systems part II: syntheses of 4-(p-substituted) phenyl-2- (2-pyrido-5-yl and 5-pyrazolo-4-yl) azo-thiazole derivatives," Dyes Pigm., vol. 63, pp. 1–9, 2004.
[55] I.Zadrożna and E. Kaczorowska, "Synthesis and characteristics of azo chromophores for nonlinear-optical application," Dyes Pigm., vol. 71, pp. 207–211, 2006.
[56] A.T. Peters and S. S. Yang, "Monoazo disperse dyes derived from mononitro-dichloro-2-aminobenzothiazoles," Dyes Pigm., vol. 30, pp. 291–299, 1996.
[57] G.Hallas and A. D. Towns, "A comparison of the properties of some 2-aminothiophene-derived disperse dyes," Dyes Pigm., vol. 31, pp. 273–289, 1996
[58] A.T. Peters and S. S. Yang, "Monoazo disperse dyes derived from nitro-2-aminobenzothiazoles," Dyes Pigm., vol. 28, pp. 151–164, 1995.
[59] G.Hallas and J. H. Choi, "Synthesis and spectral properties of azo dyes derived from 2-aminothiophenes and 2-aminothiazoles,"Dyes Pigm., vol. 42, pp. 249–265, 1999.